2024 IEEE/RSJ International Conference on Intelligent Robots and Systems (IROS)
October 14-18, 2024. Abu Dhabi, UAE

MUP-LIO: Mapping Uncertainty-aware Point-wise Lidar Inertial Odometry

Hekai Yao[1], Xuetao Zhang[1*], *IEEE Member*, Gang Sun[1], Yisha Liu[2], *IEEE Member*,
Xuebo Zhang[3], *IEEE Senior Member*, Yan Zhuang[1], *IEEE Senior Member*

***Abstract*— This paper proposes a mapping uncertainty-aware point-wise Lidar Inertial Odometry (LIO), which synthesizes the point-wise point-to-plane match and map refreshment into a probabilistic model. As a result, it can address the issue of mismatching during point registration and remove in-frame motion distortion of Lidar sensors. Specifically, the uncertainty-aware map is designed to embody the uncertainty of map geometric features (points and planes), which comes from the Lidar point measurement and pose estimation. Then the map can be modeled in a probabilistic form. In addition, the proposed framework refreshes map at each Lidar point measurement to timely revise geometric features and provide non-delayed map. On the basis, the probabilistic point-to-plane match method is designed to seek a corresponding plane for each Lidar point in point registration, which can enhance the effectiveness of match and provide adaptive observation noises for more accurate state estimation. Comparative experiments on various public datasets are conducted to demonstrate the superior performance of the proposed framework in terms of higher accuracy and better robustness.**

I. INTRODUCTION

The Simultaneous Localization and Mapping (SLAM) system [1]–[5] is the core of many robot-related tasks, such as robotic exploration and inspection [6]–[9]. The tightly coupled SLAM systems based on 3D Light Detection and Ranging (Lidar) and Inertial Measurement Unit (IMU) sensors have gained popularity due to high accuracy and robustness. In general circumstances, the systems employing an optimization framework often suffer from high computational cost, which limits their real-time applicability. To address this problem, utilizing Kalman Filter [10]–[12] for fusing Lidar and IMU data can significantly enhance calculation efficiency and increase the odometry output rate.

The accuracy and robustness of Lidar-Inertial-Odometry (LIO) systems rely heavily on an effective point cloud registration method and a valid mapping scheme. On the one hand, point cloud registration is responsible for estimating the transformation between a source point cloud and a target map by aligning them together [13]. The mapping scheme, on the other hand, plays a crucial role as it is closely intertwined with point cloud registration. It is responsible for maintaining an accurate and efficient representation of the environment through map construction and refreshment. In addition, an entire scan of point cloud data can not be measured by Lidar simultaneously, which leads to in-frame motion distortion. Addressing this distortion is essential for achieving more accurate pose estimation and map construction. Although some studies have focused on these issues, there are still some unresolved problems as follows:

- Most existing LIO systems refresh map and update system state scan-by-scan, which may cause incorrect point registration due to the delayed map and state information. In addition, the in-frame motion distortion for Lidar sensors can not be completely eliminated.
- In point registration, the existing systems tend to ignore the uncertainty of Lidar point measurement and pose estimation, utilizing predefined observation noises. Therefore, point-to-plane mismatch and imprecise state update may be caused, which affects the accuracy of pose estimation and map construction.

A. Contributions

To address the above mentioned issues, we propose a mapping uncertainty-aware point-wise LIO incorporating probabilistic point-to-plane match and non-delayed map refreshment. The uncertainty of Lidar point measurement and pose estimation is embodied within the map features in the probabilistic form, which includes points and planes with covariance. At the same time, the point-wise state update and map refreshment are performed at each Lidar point measurement. Based on this, the probabilistic point-to-plane match method is designed, where adaptive observation noises can be obtained. Then residual computation and state update are conducted with the noises. In addition, by sequentially processing each Lidar point at its respective time, Lidar in-frame motion distortion can be effectively removed. The contributions of this paper are summarized as follows:

- We propose a mapping uncertainty-aware point-wise LIO framework incorporating probabilistic match and non-delayed map refreshment methods, which can probabilistically refresh map geometric features in a point-wise manner. As a result, the non-delayed map is provided for more accurate point registration. In addition,

This work was supported in part by the National Natural Science Foundation of China under Grant 62103077, Grant U22B2041, and Grant U23A20384; in part by the Aeronautical Science Foundation of China under Grant 2022Z022063001; and in part by the Natural Science Foundation of Liaoning Province under Grant 2022-KF-12-05. *(Corresponding author: Xuetao Zhang.)*

[1]Hekai Yao, Xuetao Zhang, Gang Sun, Yan Zhuang are with the Intelligent Robotic Laboratory, School of Artificial Intelligence, also School of Control Science and Engineering, Dalian University of Technology, Dalian 116024, China. 441194403@mail.dlut.edu.cn, zhangxuetao@dlut.edu.cn,sungang@mail.dlut.edu.cn,zhuang@dlut.edu.cn

[2]Yisha Liu is with the School of Information Science and Technology, Dalian Maritime University, Dalian 116026, China. liuyisha@dlmu.edu.cn

[3]Xuebo Zhang is with the College of Artificial Intelligence, the Institute of Robotics and Automatic Information System (IRAIS), Tianjin Key Laboratory of Intelligent Robotics, Nankai University, Tianjin 300350, China. zhangxuebo@nankai.edu.cn

updating state at each Lidar point measurement can also eliminate Lidar in-frame motion distortion.
- A novel probabilistic point-to-plane match method for point-wise LIO framework is designed, which accounts for the uncertainty associated with Lidar point measurement, pose estimation and map geometric features. Therefore, mismatches can be reduced and adaptive observation noises can be obtained for more accurate state update.
- We implement the LIO framework and evaluate the superior performance through various experiments under public datasets. The proposed method outperforms three state-of-the-art methods in terms of accuracy and robustness.

II. RELATED WORK

The Lidar-IMU tightly coupled SLAM systems have garnered increasing attention in recent years. The detailed explanation of the IMU pre-integration model is provided in [14], which has served as the basis for numerous LIO-related methods employing an optimization framework, such as [15]–[20]. The LIO system proposed in [21], [22] estimates B-spline-based continuous-time trajectory instead of discrete trajectory points, which can facilitate the easy fusion of asynchronous sensor data. However, these systems have significant computational consumption. To address the problem, LIO systems based on Kalman Filter have been investigated in the recent few years [10]–[12].

The point cloud registration and mapping scheme are two necessary modules, which are interdependent. Some systems such as LOAM [23] and LEGO-LOAM [24] tend to extract geometric features and perform scan-to-scan registration. The method can result in the accumulation of registration errors between scans. In contrast, direct methods like [10]–[12] can directly register the point cloud to the target map. However, the registration results may be affected by the Lidar in-frame motion distortion. To address this issue, POINT-LIO [12] proposes a point-by-point LIO framework that directly registers a raw Lidar point into the target map. However, POINT-LIO ignores the uncertainty of the Lidar point measurement and pose estimation, utilizing predefined observation noises, which may cause inaccurate point-to-plane match, affecting the LIO system accuracy.

For the mapping scheme, a common approach is to represent the point cloud map using a kd-tree structure [23], [24]. However, the map refreshment is time-consuming. Therefore, the ikd-tree [25] is utilized to efficiently organize and refresh the point cloud map in [11]. However, the uncertainty of map geometric features is not considered. Other methods such as [13], [26]–[28] employ hash-based voxels element to store and represent the target map. In particular, the uncertainty of map features is modeled in [27], [28]. The aforementioned mapping methods typically refresh the map scan-by-scan. However, inserting a Lidar point into the map will have an impact on the point-to-plane match process for the remaining points in the same scan and the points in subsequent scans. Therefore, the aforementioned methods can not be applied to the point-wise LIO framework, as they may result in incorrect registration due to the delayed map.

Motivated by above discussion, this paper proposes a point-wise LIO framework, where the probabilistic point registration and non-delayed map refreshment method are designed. The framework considers the uncertainty from Lidar point measurement, pose estimation and the map in point registration, which can reduce the incorrect point-to-plane match. The designed probabilistic point-to-plane method can also provide adaptive observation noises for state update. In addition, the map is non-delayed due to the point-wise refreshment scheme.

The remainder of this paper is organized as follows: Section III-A provides an overview of the proposed framework. Section III-B details the point-wise state estimation method. In addition, map refreshment scheme in uncertainty-aware mapping is illustrated in III-C. To demonstrate the superior performance of the proposed method, the results of our experiments are presented in Section IV. The conclusion section is presented in the end.

III. METHODOLOGY

In this section, the overview of the proposed system is described at first. Then the point-wise state estimation method is detailed, which includes *Kinematic Model*, *Probabilistic Point-to-Plane Match* and *Extended Kalman Filter Update*. Additionally, *Point-wise Map Refreshment* in uncertainty-aware mapping method is explained in the end.

A. System Overview

The proposed LIO system framework is shown in Fig.1, consisting of two main modules: point-wise state estimation and uncertainty aware mapping. The first Lidar scan is used to construct an initial probabilistic map. The subsequent Lidar data is divided into each individual point at their respective times, and the point is sent into the point-wise state estimation module with propagated state. In point-wise state estimation module, the point uncertainty in global frame will be evaluated with the pose estimation uncertainty. After this, with the uncertainty-aware map, probabilistic boundary point-to-plane match is conducted to provide constrain for updating state and covariance. At last, the updated point can be registered to refresh map and revise uncertainty of geometric features, which can produce non-delayed map in the point-wise manner. In addition, if no corresponding plane can be found in the established map during point registration, the point need to be inserted into map with propagated state. As for each IMU data, the processing follows approach with in [12].

B. Point-wise State Estimation

1) Kinematic Model: This section describes Kinematic Model. To facilitate understanding, the notations mentioned in this paper are listed in Table I. These notations will be used to clarify the concepts and equations involved in point-wise state estimation.

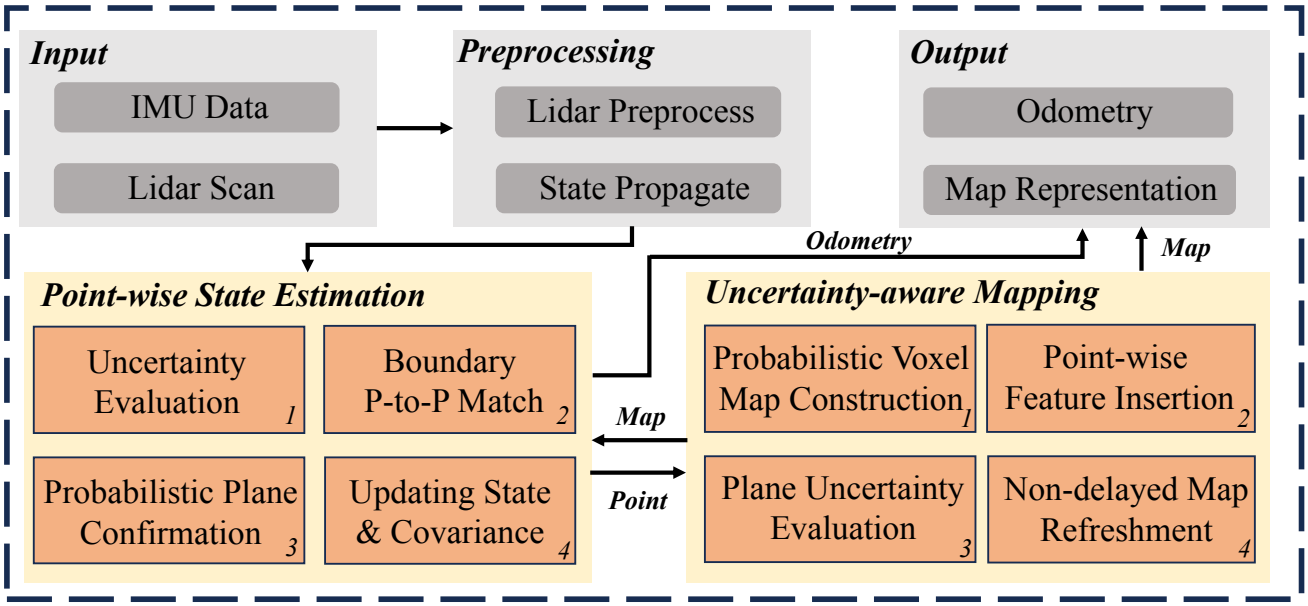

Fig. 1. System framework.

TABLE I
SOME IMPORTANT NOTATIONS

Symbols	Meanings
$\mathbf{x}, \hat{\mathbf{x}}, \bar{\mathbf{x}}$	The ground-truth, propagated, and updated state $\mathbf{x}$.
$\mathbf{x}_k$	State $\mathbf{x}$ at the k-th measurement sampling time.
$\mathbf{T}$	Sensor pose including position $\mathbf{p}$ and rotation $\mathbf{R}$.
δx	Error compared to ground-truth state $\mathbf{x}$.
$\boxplus$	operations in manifold $\mathcal{M} \times \mathbb{R}^n \to \mathcal{M}$.
$\mathbf{J}_\alpha$ and $\mathbf{H}_\alpha$	Partial differentiation operation respect to α evaluated at zero.

In the proposed system, the IMU frame is defined as the body frame (denoted as I), and the first IMU frame is considered as the global frame (denoted as G). With this frame setup, the discretized state transition model can be expressed as follows:

$$\mathbf{x}_{k+1} = \mathbf{x}_k \boxplus (\Delta t_k \mathbf{f}(\mathbf{x}_k, \mathbf{w}_k)) \tag{1}$$

where k is the k-th measurement sampling time, Δt_k is the time interval since the last measurement. Function $\mathbf{f}$, state $\mathbf{x}$, and noises $\mathbf{w}$ are defined as follows:

$$\begin{aligned}
\mathcal{M} &\triangleq \mathrm{SO}(3) \times \mathbb{R}^{21}, \dim(\mathcal{M}) = 24 \\
\mathbf{x} &\triangleq [{}^G\mathbf{R}_I \quad {}^G\mathbf{p}_I \quad {}^G\mathbf{v}_I \quad \mathbf{b}_g \quad \mathbf{b}_a \quad {}^G\mathbf{g} \quad {}^I\boldsymbol{\omega} \quad {}^I\mathbf{a}] \\
\mathbf{w} &\triangleq [\mathbf{n}_{\mathrm{b_g}} \quad \mathbf{n}_{\mathrm{b_a}} \quad \mathbf{w}_{\mathrm{g}} \quad \mathbf{w}_{\mathrm{a}}] \sim \mathcal{N}(\mathbf{0}, \mathcal{Q}) \\
\mathbf{f}(\mathbf{x}, \mathbf{w}) &\triangleq [{}^I\boldsymbol{\omega} \quad {}^G\mathbf{v}_I \quad {}^G\mathbf{R}_I \cdot {}^I\mathbf{a} + {}^G\mathbf{g} \quad \mathbf{n}_{\mathbf{b}_g} \quad \mathbf{n}_{\mathbf{b}_a} \\
&\qquad \mathbf{0}_{3\times 1} \quad \mathbf{w}_{\mathrm{g}} \quad \mathbf{w}_{\mathrm{a}}] \in \mathbb{R}^{24}
\end{aligned} \tag{2}$$

where ${}^G\mathbf{R}_I$, ${}^G\mathbf{p}_I$, and ${}^G\mathbf{v}_I$ are the global attitude, position, and velocity of the IMU. $\mathbf{b}_g$ and $\mathbf{b}_a$ are IMU biases with Gaussian noises $\mathbf{n}_{\mathbf{b_g}} \sim \mathcal{N}(\mathbf{0}, \mathcal{Q}_{\mathrm{b_g}})$ and $\mathbf{n}_{\mathbf{b_a}} \sim \mathcal{N}(\mathbf{0}, \mathcal{Q}_{\mathrm{b_a}})$, ${}^G\mathbf{g}$ is the global gravity, the ${}^I\boldsymbol{\omega}$ and ${}^I\mathbf{a}$ are angular velocity and linear acceleration along with noises $\mathbf{w_g} \sim \mathcal{N}(\mathbf{0}, \mathcal{Q}_{\mathrm{g}})$,$\mathbf{w_a} \sim \mathcal{N}(\mathbf{0}, \mathcal{Q}_{\mathrm{a}})$, and Q =diag$(Q_{\mathrm{b_g}}, Q_{\mathrm{b_a}}, Q_{\mathrm{g}}, Q_{\mathrm{a}})$ is the covariance matrix of the process noise $\mathbf{w}$.

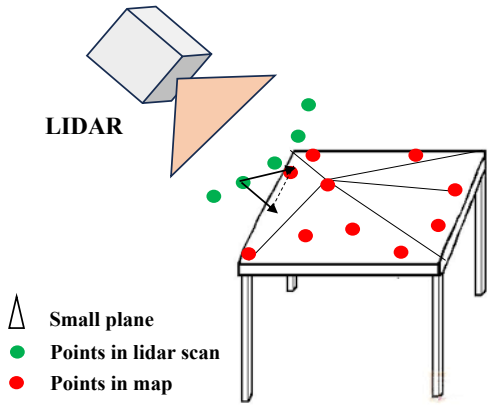

Fig. 2. Illustration of the observation model.

Regarding the observation model, once projected into the global frame using the ground-true IMU pose, each lidar point is expected to lie precisely on a local small plane within the global map, as illustrated in Fig.2. Based on this, observation model can be deduced as follows:

$$0 = ({}^G\mathbf{u}_k^{gt})^\top ({}^G\mathbf{T}_{I_k}^{gt} {}^I\mathbf{p}_{\mathbf{m}_k}^{gt} - {}^G\mathbf{q}_k^{gt}) \tag{3}$$

where ${}^G\mathbf{u}_k^{gt}$ is normal vector of the corresponding plane without noises, and ${}^G\mathbf{q}_k^{gt}$ is a point in the plane. ${}^G\mathbf{T}_{I_k}^{gt}$ is IMU pose implicit in state $\mathbf{x}_k$. ${}^I\mathbf{p}_{\mathbf{m}_k}^{gt}$ is a ground-truth Lidar point in IMU frame (the Lidar frame and the IMU frame should have precalibrated extrinsic). It is worth mentioning that the IMU observation model and state update method

follow the same principles in [12]. Therefore, no detailed definitions and derivations are described here. Furthermore, the observation model $\mathbf{h}_{\mathrm{L}}$ for Lidar described in equation (3) can be written in a compact form as

$$0 = \mathbf{h}_{\mathrm{L}}(\mathbf{x}_k, {}^{G}\mathbf{u}_k^{gt}, {}^{I}\mathbf{p}_{\mathrm{m}_k}^{gt}, {}^{G}\mathbf{q}_k^{gt}) \tag{4}$$

2) Probabilistic Point-to-Plane Match: As shown in Fig.3, the map of the proposed system is composed of voxels organized using a Hash table and octrees [27]. Each voxel within the map contains a map plane feature and some map points, which also includes their uncertainty. The map can provide a probabilistic representation of the environment by incorporating uncertainties of each Lidar point measurement and pose estimation. By the way, the uncertainties of pose estimation in tangent space are expressed in covariance matrix $\mathbf{P}$.

When a new Lidar point ${}^{G}\mathbf{p}_i$ is projected into global frame with its propagated pose, point-to-plane match is conducted to provide constraints for state update. Assume that there is a plane with a normal vector ${}^{G}\mathbf{u}_i$ and a center point ${}^{G}\mathbf{q}_i$, the distance d_i between the point ${}^{G}\mathbf{p}_i$ and the plane is as follows:

$$d_i = {}^{G}\mathbf{u}_i^{\top}({}^{G}\mathbf{p}_i - {}^{G}\mathbf{q}_i) \tag{5}$$

Consider the uncertainty of ${}^{G}\mathbf{u}_i$, ${}^{G}\mathbf{p}_i$, ${}^{G}\mathbf{q}_i$ in global map, the point-to-plane distance is as follows:

$$\begin{aligned} d_i =& ({}^{G}\mathbf{u}_i^{gt} \boxplus \delta_{G\mathbf{u}_i})^{\top}[({}^{G}\mathbf{p}_i^{gt} + \delta_{G\mathbf{p}_i}) - {}^{G}\mathbf{q}_i^{gt} - \delta_{G\mathbf{q}_i}] \\ \approx& \underbrace{({}^{G}\mathbf{u}_i^{gt})^{\top}({}^{G}\mathbf{p}_i^{gt} - {}^{G}\mathbf{q}_i^{gt})}_{a} \\ &+ \mathbf{J}_{G\mathbf{u}_i}\delta_{G\mathbf{u}_i} + \mathbf{J}_{G\mathbf{q}_i}\delta_{G\mathbf{q}_i} + \mathbf{J}_{G\mathbf{p}_i}\delta_{G\mathbf{p}_i} \end{aligned} \tag{6}$$

From the observation model in equation (3), the part a in equation (6) is zero and this implies that $d_i \sim \mathcal{N}(0, \Sigma_{\mathbf{w}_i})$ if we denote $\mathbf{w}_i = \mathbf{J}_{G\mathbf{u}_i}\delta_{G\mathbf{u}_i} + \mathbf{J}_{G\mathbf{q}_i}\delta_{G\mathbf{q}_i} + \mathbf{J}_{G\mathbf{p}_i}\delta_{G\mathbf{p}_i}$ and

$$\begin{aligned} \Sigma_{\mathbf{w}_i} &= \mathbf{J}_{\mathbf{w}_i}\boldsymbol{\Sigma}_{G\mathbf{u}_i, G\mathbf{q}_i, G\mathbf{p}_i}\mathbf{J}_{\mathbf{w}_i}^{\top} \\ \mathbf{J}_{\mathbf{w}_i} &= \left[\mathbf{J}_{G\mathbf{u}_i}, \mathbf{J}_{G\mathbf{q}_i}, \mathbf{J}_{G\mathbf{p}_i}\right] \\ &= \left[({}^{G}\mathbf{p}_i - {}^{G}\mathbf{q}_i)^{\top}, -{}^{G}\mathbf{u}_i^{\top}, {}^{G}\mathbf{u}_i^{\top}\right] \\ \boldsymbol{\Sigma}_{G\mathbf{u}_i, G\mathbf{q}_i, G\mathbf{p}_i} &= \begin{bmatrix} \boldsymbol{\Sigma}_{G\mathbf{u}_i, G\mathbf{q}_i} & 0 \\ 0 & \boldsymbol{\Sigma}_{\mathbf{G}\mathbf{p}_i} \end{bmatrix} \end{aligned} \tag{7}$$

where $\boldsymbol{\Sigma}_{G\mathbf{u}_i, G\mathbf{q}_i}$ and $\boldsymbol{\Sigma}_{\mathbf{G}\mathbf{p}_i}$ are the covariance of the plane and the Lidar point in global map referenced from [27].

According to the above analysis, when a point is effectively matched to a plane, the distance between them is expected to fall within a range of 3σ, where σ=$\sqrt{\Sigma_{\mathbf{w}_i}}$. This range is determined by the uncertainty in the observation. In the case where multiple planes are matched to a same point, the plane with the highest probability will be selected. If none of the planes pass the probabilistic distance filtering, the point will be inserted directly into the map using its propagated prior pose information.

3) Extended Kalman Filter Update: Assuming the system has obtained the updated state estimation $\bar{\mathbf{x}}_{k\text{-}1}$ up to sampling time k-1 with the corresponding updated covariance matrix

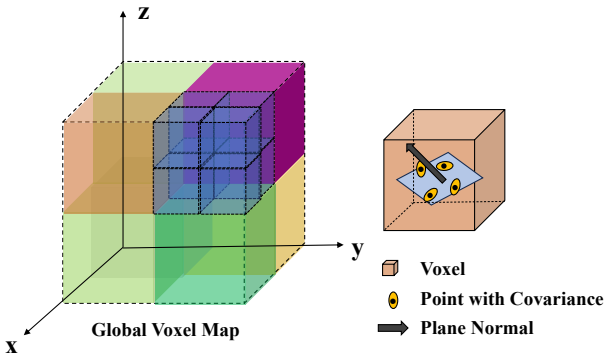

Fig. 3. Map structure of our system. The map is a collection of voxels organized by a Hash table and octrees, each contains some points, a plane center and the plane normal.

$\bar{\mathbf{P}}_{k\text{-}1}$, the state propagation model described in [12] is utilized to obtain the state estimation prior $\hat{\mathbf{x}}_k$ along with its covariance matrix $\hat{\mathbf{P}}_k$.

By combining the probabilistic point-to-plane match method discussed in III-B-(2), the Maximum A Posterior (MAP) estimate of the system state can be obtained. Specifically, for an effective point-to-plane match, the observation equation can be written as

$$\begin{aligned} \mathbf{r}_k &= \mathbf{h}_{\mathrm{L}}(\mathbf{x}_k, {}^{G}\mathbf{u}_k^{gt}, {}^{I}\mathbf{p}_{\mathrm{m}_k}^{gt}, {}^{G}\mathbf{q}_k^{gt}) + \mathbf{v}_k \\ &= \mathbf{h}_{\mathrm{L}}(\mathbf{x}_k, {}^{G}\mathbf{u}_k, {}^{I}\mathbf{p}_{\mathrm{m}_k}, {}^{G}\mathbf{q}_k) \\ &= {}^{G}\mathbf{u}_k^{\top}({}^{G}\mathbf{p}_{m_k} - {}^{G}\mathbf{q}_k) \\ &= ({}^{G}\mathbf{u}_k^{gt} \boxplus \delta_{\mathbf{u}_k})^{\top} \times \\ &\quad [({}^{G}\mathbf{T}_{I_k}^{gt} \boxplus \delta_{\mathbf{T}_{I_k}})({}^{I}\mathbf{p}_{m_k}^{gt} + \delta_{\mathbf{p}_{m_k}}) - {}^{G}\mathbf{q}_k^{gt} - \delta_{\mathbf{q}_k}] \\ &\approx \underbrace{({}^{G}\mathbf{u}_k^{gt})^{\top}({}^{G}\mathbf{T}_{I_k}^{gt}\,{}^{I}\mathbf{p}_{m_k}^{gt} - {}^{G}\mathbf{q}_k^{gt})}_{a} \\ &\quad + \mathbf{J}_{G\mathbf{T}_{I_k}}\delta_{G\mathbf{T}_{I_k}} \\ &\quad + \mathbf{J}_{G\mathbf{u}_k}\delta_{G\mathbf{u}_k} + \mathbf{J}_{G\mathbf{q}_k}\delta_{G\mathbf{q}_k} + \mathbf{J}_{I\mathbf{p}_{m_k}}\delta_{I\mathbf{p}_{m_k}} \end{aligned} \tag{8}$$

where the $\mathbf{r}_k$ is point-to-plane distance residual. And the observation noises $\mathbf{v}_k \sim (\mathbf{0}, \mathbf{U}_k)$ can be automatically calculated. The part a in equation (8) is zero, then $\mathbf{J}_{G\mathbf{T}_{I_k}}\delta_{G\mathbf{T}_{I_k}}$ can be written as corresponding $\mathbf{H}_{\mathbf{x}_k}\delta_{\mathbf{x}_k}$ since the IMU pose $\mathbf{T}$ is contained in state vector $\mathbf{x}$. Additionally, $\mathbf{U}_k = \mathbf{J}_{\mathbf{v}_k}\boldsymbol{\Sigma}_{G\mathbf{u}_k, G\mathbf{q}_k, I\mathbf{p}_{m_k}}\mathbf{J}_{\mathbf{v}_k}^{\top}$ can be deduced from equation (8) and

$$\begin{aligned} \mathbf{J}_{\mathbf{v}_k} &= [\mathbf{J}_{G\mathbf{u}_k}, \mathbf{J}_{G\mathbf{q}_k}, \mathbf{J}_{I\mathbf{p}_{m_k}}] \\ &= [({}^{G}\bar{\mathbf{T}}_{I_k}\,{}^{I}\mathbf{p}_{m_k} - {}^{G}\mathbf{q}_k)^{\top}, -{}^{G}\mathbf{u}_k^{\top}, {}^{G}\mathbf{u}_k^{\top}\bar{\mathbf{R}}_k] \\ \boldsymbol{\Sigma}_{G\mathbf{u}_k, G\mathbf{q}_k, I\mathbf{p}_{m_k}} &= \begin{bmatrix} \boldsymbol{\Sigma}_{G\mathbf{u}_k, G\mathbf{q}_k} & 0 \\ 0 & \boldsymbol{\Sigma}_{I\mathbf{p}_{m_k}} \end{bmatrix} \end{aligned} \tag{9}$$

By combining state prior with the valid point-to-plane match constraint, the MAP estimation of state $\bar{\mathbf{x}}_k$ represented by $\delta\mathbf{x}_k$ is as follows:

$$\underset{\delta\mathbf{x}_k}{\operatorname{argmin}}(\|\mathbf{r}_k - \mathbf{H}_{x_k}\delta\mathbf{x}_k\|_{\mathbf{U}_k}^2 + \|\delta\mathbf{x}_k\|_{\hat{\mathbf{P}}_k}^2) \tag{10}$$

The first part is from observation model and the second part is from the propagated state prior, $\|\mathbf{x}\|_{\mathbf{A}}^2 = \mathbf{x}^{\top}\mathbf{A}^{-1}\mathbf{x}$.

Then $\bar{\mathbf{x}}_k = \hat{\mathbf{x}}_k \boxplus \delta\mathbf{x}_k^*$, where $\delta\mathbf{x}_k^*$ is optimal solution of (10). The updated covariance $\bar{\mathbf{P}}_k$ can be calculated similarly to standard Kalman update.

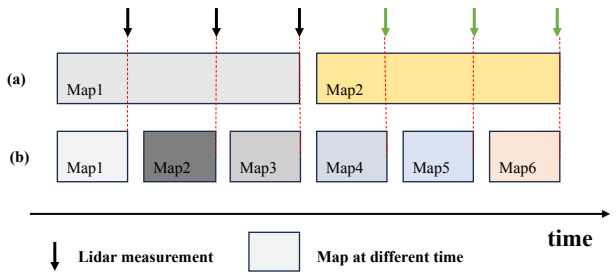

Fig. 4. The different map refreshment schemes. Arrows of the same color represent point clouds from the same scan of the Lidar measurement. The map is displayed with colors that change over time and with Lidar measurements. (a) is scan-by-scan map refreshment scheme.(b) is point-by-point map refreshment scheme.

C. Point-wise Map Refreshment

In the designed framework, the point-to-plane match and subsequent state update step are executed point by point. With the updated or propagated pose, each Lidar point is registered into the global map to refresh the map. Fig.4 illustrates this process. The arrows with the same color represent Lidar point measurement from the same Lidar scan, and the color change indicates the map refreshment process over time. There are two map refreshment methods:

For the first method (a), when the black scan is being processed, each point searches for its corresponding plane in the same *Map1*. The map is refreshed to *Map2* only when the last Lidar measurement point in this scan is processed. However, registering one point into the map may influence the matching results for its subsequent point during the point-to-plane match process. To address this issue and get more accurate match results, the point-wise map refreshment strategy shown in (b) is designed, the map is refreshed point by point in chronological order, which can provide a non-delayed map for more accurate point-to-plane match during point registration.

IV. EXPERIMENT

In this section, comparative experiments are conducted to evaluate the performance of the proposed method in various scenarios, including campus environment and challenging scenes. To evaluate the accuracy of the proposed system, Root Mean Square Error (RMSE, meters) of Absolute Pose Error (APE) is chosen as evaluation metric [29]. Three state-of-the-art systems are compared with our system: FAST-LIO2 [11], which is a fast, robust, and versatile LIO framework based on a highly efficient tightly-coupled iterated Kalman Filter; PV-LIO, the IMU version of [27] open sourced on Github; POINT-LIO [12], a robust and high-bandwidth LIO, which is capable of estimating extremely aggressive robotic motions.

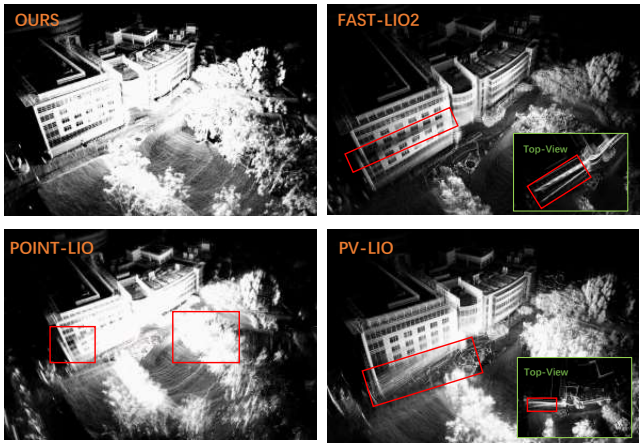

Fig. 5. The mapping result of different methods on spms-01 sequence.

TABLE II
RMSE(METERS) OF ABSOLUTE POSE ERRORS IN EACH SEQUENCE ON NTU-VIRAL DATASET.

Sequence	OURS	POINT-LIO	FAST-LIO2	PV-LIO
rtp-01	**0.164193**	0.822245	0.212089	0.287835
rtp-02	**0.122686**	0.163191	0.153968	0.934816
rtp-03	**0.167994**	0.19854	0.194075	0.302795
nya-01	0.172654	0.217402	**0.168079**	0.426442
nya-02	**0.169649**	0.215078	0.177101	0.381465
nya-03	**0.166027**	0.181894	0.178661	0.675788
eee-01	0.168155	0.188277	**0.158396**	4.112456
eee-02	**0.149097**	0.153966	0.169953	1.193780
eee-03	0.191080	0.197222	**0.179234**	0.465292
spms-01	**0.249991**	1.186950	1.827605	1.810679
spms-02	**0.460770**	0.581459	3.628222	2.073493
spms-03	**0.174562**	0.499331	0.762167	Fail
sbs-01	0.188178	0.191895	**0.183802**	1.015116
sbs-02	0.188612	0.198764	**0.186571**	0.210156
sbs-03	0.179076	0.183573	**0. 176288**	0.567280
Average	**0.194182**	0.345319	0.557081	1.032671

All experiments are conducted in the Robots Operating System (ROS) on a computer with an Intel i9-13900K processor running at 5.80 GHz and 32 GB of RAM. It is worth mentioning that the parameters of all these methods are consistent across the experiments, except some unshared parameters that are kept the default in their respective open releases.

1) Campus Experiments: The accuracy evaluation experiments of our system are under the public dataset NTU-VIRAL [30], which is collected from an Unmanned Aerial Vehicle (UAV) platform at Nanyang Technological University. The dataset consists of both indoor and outdoor scenes within the university campus. It includes sensor data from

TABLE III
RMSE(METERS) OF ABSOLUTE POSE ERRORS ON CHALLENGING SCENES.

Method	room-01	door-01	door-02	gate-01	urban-01	urban-02
POINT-LIO	**0.397748**	0.462816	0.331513	0.124248	1.775369	1.649443
FAST-LIO2	0.408284	0.470821	0.343297	0.130236	1.636718	**1.147900**
PV-LIO	0.399150	0.472770	0.331874	0.123611	1.355935	1.214043
OURS	0.398201	**0.442505**	**0.310980**	**0.113751**	**1.308917**	1.339033
SCENE	Narrow room, short-term	Outdoor to indoor to outdoor, long-term	Outdoor to indoor, short-term	Campus gate, short-term	Urban street, long-term	Urban street, long-term
CHALLENGING	Unstructured	Scene change	Scene change	Dynamic	Dynamic	Dynamic

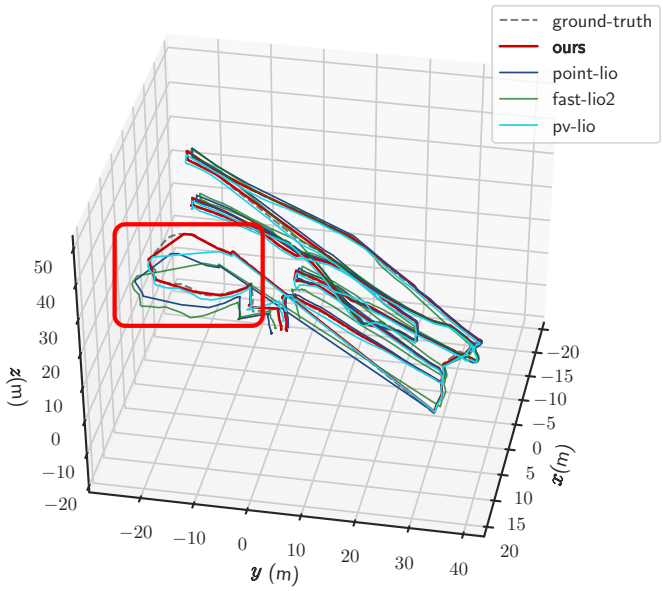

Fig. 6. Trajectories reference to the ground-truth on sequence spms-01.

two 16-beam Ouster Lidars operating at 10 Hz, a VectorNav VN100 IMU operating at 385 Hz. This dataset provides a comprehensive and diverse set of data for evaluating and validating the performance of the proposed system in real-world scenarios.

Table II displays the results of the RMSE for all methods evaluated. The best results are highlighted in bold. It is evident from the table that our method achieves the best average RMSE 0.194182m,where the failed sequences are not included when calculating the average. In most environments, our system outperforms all other algorithms in terms of accuracy, particularly in challenging scenarios such as the spms sequences. It is worthwhile to note that the dataset on spms-01 sequence is one of the difficult sequences, where the environment is full of unstructured trees and the UAV moves fast. To further demonstrate the high accuracy of proposed method, the mapping result of spms-01 sequence is presented in Fig.5. As can be observed, more point can be reserved due to the point-wise point-to-plane match and our method performs better in the mixed environment of buildings and trees. The subtle structure of the trees is accurately reconstructed and there is no blur on the walls in contrast to the other three state-of-the-art methods. In addition, the trajectories reference to the ground-truth on NTU-viral dataset spms-01 sequence for all methods are shown in Fig.6 and emphasized by the red box. Our trajectory is closest to ground-truth when the UAV performs large-angle turns, proving the improved performance.

The improved performance can be primarily attributed to the proposed uncertainty-aware point-wise LIO framework and the probabilistic point-to-plane match method. Based on the map modeled in a probabilistic form, the accuracy of the point-to-plane match in point registration is enhanced, which can provide more precise constrain for state update. In addition, by updating the system state at each Lidar point measurement, Lidar in-frame motion distortion can be effectively removed.

2) Challenging Scene Experiments: In order to validate the robustness and applicability of the proposed framework in complex environments, the results of experiments under challenging datasets obtained from M2DGR [31] and Urban-Loco [32] are listed in Table III. The room-01 sequence was collected in a narrow, messy and unstructured room using a handheld device, making it prone to get incorrect point-to-plane match result. The door-01 and door-02 sequences contain scenes involving indoor and outdoor switching. The narrow doorway presents challenges as it can result in unavailability of already established map. The remaining three sequences involve scenarios with moving vehicles and pedestrians, posing challenges for the system due to incorrect map features in such dynamic environments. These datasets are chosen to evaluate the performance of our method in handling these challenging scenarios.

Table III presents the RMSE (meters) results of the experiments. The best results are highlighted in bold. These experimental results demonstrate that the proposed framework performs better in terms of accuracy under these challenging scenes, confirming the robustness simultaneously. The proposed point-wise uncertainty-aware mapping method can refresh map and their uncertainty at each Lidar point, which

ensures that map features can be promptly supplemented and updated, providing non-delayed map for more accurate point registration, especially during fast movement and scene switching.

It is worth mentioning that, although our method requires processing thousands of points, it does not affect its real-time performance.

CONCLUSION

In conclusion, this paper proposes a mapping uncertainty-aware point-wise LIO system. Unlike most of the existing methods, the framework designs a probabilistic point-to-plane matching method during point registration in point-wise LIO. To address the problem of Lidar in-frame motion distortion, point-wise state update and map refreshment methods at each Lidar point measurement are proposed, which can also provide the system with a non-delayed map for more accurate registration. The superior performance of the proposed method is demonstrated through comparative experiments on various public datasets. In the future, we will improve our method to enhance robustness in some extreme geometrically uninformative environments, such as mines.

REFERENCES

[1] H. Shen, Q. Zong, B. Tian, and H. Lu, "Voxel-based localization and mapping for multirobot system in gps-denied environments," *IEEE Transactions on Industrial Electronics*, vol. 69, no. 10, pp. 10 333–10 342, 2022.

[2] J. Zhang, H. Zhuge, Z. Wu, G. Peng, M. Wen, Y. Liu, and D. Wang, "4dradarslam: A 4d imaging radar slam system for large-scale environments based on pose graph optimization," in *2023 IEEE International Conference on Robotics and Automation (ICRA)*, 2023, pp. 8333–8340.

[3] Y. Chen, J. Cheng, L. Gan, S. Wang, H. Liu, X. Mei, and M. Liu, "Ir-stp: Enhancing autonomous driving with interaction reasoning in spatio-temporal planning," *IEEE Transactions on Intelligent Transportation Systems*, pp. 1–13, 2024.

[4] B. Li, D. Zou, Y. Huang, X. Niu, L. Pei, and W. Yu, "Textslam: Visual slam with semantic planar text features," *IEEE Transactions on Pattern Analysis and Machine Intelligence*, vol. 46, no. 1, pp. 593–610, 2024.

[5] J. Li, X. Pan, G. Huang, Z. Zhang, N. Wang, H. Bao, and G. Zhang, "Rd-vio: Robust visual-inertial odometry for mobile augmented reality in dynamic environments," *IEEE Transactions on Visualization and Computer Graphics*, pp. 1–14, 2024.

[6] Q. Bi, X. Zhang, J. Wen, Z. Pan, S. Zhang, R. Wang, and J. Yuan, "Cure: A hierarchical framework for multi-robot autonomous exploration inspired by centroids of unknown regions," *IEEE Transactions on Automation Science and Engineering*, pp. 1–14, 2023.

[7] S. Zhang, R. Cui, W. Yan, and Y. Li, "Dual-layer path planning with pose slam for autonomous exploration in gps-denied environments," *IEEE Transactions on Industrial Electronics*, vol. 71, no. 5, pp. 4976–4986, 2024.

[8] Z. Zhang, Y. Chen, F. Han, J. Fan, H. Yu, H. Zhang, and Y. Wang, "Wgit*: Workspace-guided informed tree for motion planning in restricted environments," *IEEE/ASME Transactions on Mechatronics*, pp. 1–12, 2024.

[9] X. Zhang, X. Xu, Y. Liu, H. Wang, X. Zhang, and Y. Zhuang, "Fgip: A frontier-guided informative planner for uav exploration and reconstruction," *IEEE Transactions on Industrial Informatics*, pp. 1–12, 2023.

[10] W. Xu and F. Zhang, "Fast-lio: A fast, robust lidar-inertial odometry package by tightly-coupled iterated kalman filter," *IEEE Robotics and Automation Letters*, vol. 6, no. 2, pp. 3317–3324, 2021.

[11] W. Xu, Y. Cai, D. He, J. Lin, and F. Zhang, "Fast-lio2: Fast direct lidar-inertial odometry," *IEEE Transactions on Robotics*, vol. 38, no. 4, pp. 2053–2073, 2022.

[12] D. He, W. Xu, N. Chen, F. Kong, C. Yuan, and F. Zhang, "Point-lio: Robust high-bandwidth light detection and ranging inertial odometry," *Advanced Intelligent Systems*, vol. 5, no. 7, p. 2200459, 2023.

[13] X. Ji, S. Yuan, P. Yin, and L. Xie, "Lio-gvm: an accurate, tightly-coupled lidar-inertial odometry with gaussian voxel map," *IEEE Robotics and Automation Letters*, 2024.

[14] C. Forster, L. Carlone, F. Dellaert, and D. Scaramuzza, "On-manifold preintegration for real-time visual–inertial odometry," *IEEE Transactions on Robotics*, vol. 33, no. 1, pp. 1–21, 2016.

[15] W. Dai, Y. Zhang, P. Li, Z. Fang, and S. Scherer, "Rgb-d slam in dynamic environments using point correlations," *IEEE Transactions on Pattern Analysis and Machine Intelligence*, vol. 44, no. 1, pp. 373–389, 2020.

[16] H. Gao, X. Zhang, J. Yuan, and Y. Fang, "Negl: Lightweight and efficient neighborhood encoding-based global localization for unmanned ground vehicles," *IEEE Transactions on Vehicular Technology*, vol. 72, no. 6, pp. 7111–7122, 2023.

[17] P. Geneva, K. Eckenhoff, Y. Yang, and G. Huang, "Lips: Lidar-inertial 3d plane slam," in *2018 IEEE/RSJ International Conference on Intelligent Robots and Systems (IROS)*. IEEE, 2018, pp. 123–130.

[18] C. Le Gentil, T. Vidal-Calleja, and S. Huang, "In2lama: Inertial lidar localisation and mapping," in *2019 International Conference on Robotics and Automation (ICRA)*. IEEE, 2019, pp. 6388–6394.

[19] H. Ye, Y. Chen, and M. Liu, "Tightly coupled 3d lidar inertial odometry and mapping," in *2019 International Conference on Robotics and Automation (ICRA)*. IEEE, 2019, pp. 3144–3150.

[20] T. Shan, B. Englot, D. Meyers, W. Wang, C. Ratti, and D. Rus, "Lio-sam: Tightly-coupled lidar inertial odometry via smoothing and mapping," in *2020 IEEE/RSJ international conference on intelligent robots and systems (IROS)*. IEEE, 2020, pp. 5135–5142.

[21] J. Lv, K. Hu, J. Xu, Y. Liu, X. Ma, and X. Zuo, "Clins: Continuous-time trajectory estimation for lidar-inertial system," in *2021 IEEE/RSJ International Conference on Intelligent Robots and Systems (IROS)*. IEEE, 2021, pp. 6657–6663.

[22] X. Lang, C. Chen, K. Tang, Y. Ma, J. Lv, Y. Liu, and X. Zuo, "Coco-lic: continuous-time tightly-coupled lidar-inertial-camera odometry using non-uniform b-spline," *IEEE Robotics and Automation Letters*, 2023.

[23] J. Zhang and S. Singh, "Loam: Lidar odometry and mapping in real-time." in *Robotics: Science and systems*, vol. 2, no. 9. Berkeley, CA, 2014, pp. 1–9.

[24] T. Shan and B. Englot, "Lego-loam: Lightweight and ground-optimized lidar odometry and mapping on variable terrain," in *2018 IEEE/RSJ International Conference on Intelligent Robots and Systems (IROS)*. IEEE, 2018, pp. 4758–4765.

[25] Y. Cai, W. Xu, and F. Zhang, "ikd-tree: An incremental kd tree for robotic applications," *arXiv preprint arXiv:2102.10808*, 2021.

[26] C. Bai, T. Xiao, Y. Chen, H. Wang, F. Zhang, and X. Gao, "Faster-lio: Lightweight tightly coupled lidar-inertial odometry using parallel sparse incremental voxels," *IEEE Robotics and Automation Letters*, vol. 7, no. 2, pp. 4861–4868, 2022.

[27] C. Yuan, W. Xu, X. Liu, X. Hong, and F. Zhang, "Efficient and probabilistic adaptive voxel mapping for accurate online lidar odometry," *IEEE Robotics and Automation Letters*, vol. 7, no. 3, pp. 8518–8525, 2022.

[28] C. Wu, Y. You, Y. Yuan, X. Kong, Y. Zhang, Q. Li, and K. Zhao, "Voxelmap++: Mergeable voxel mapping method for online lidar (-inertial) odometry," *IEEE Robotics and Automation Letters*, vol. 9, no. 1, pp. 427–434, 2023.

[29] M. Grupp, "evo: Python package for the evaluation of odometry and slam." https://github.com/MichaelGrupp/evo, 2017.

[30] T.-M. Nguyen, S. Yuan, M. Cao, Y. Lyu, T. H. Nguyen, and L. Xie, "Ntu viral: A visual-inertial-ranging-lidar dataset, from an aerial vehicle viewpoint," *The International Journal of Robotics Research*, vol. 41, no. 3, pp. 270–280, 2022.

[31] J. Yin, A. Li, T. Li, W. Yu, and D. Zou, "M2dgr: A multi-sensor and multi-scenario slam dataset for ground robots," *IEEE Robotics and Automation Letters*, vol. 7, no. 2, pp. 2266–2273, 2021.

[32] W. Wen, Y. Zhou, G. Zhang, S. Fahandezh-Saadi, X. Bai, W. Zhan, M. Tomizuka, and L.-T. Hsu, "Urbanloco: A full sensor suite dataset for mapping and localization in urban scenes," in *2020 IEEE international conference on robotics and automation (ICRA)*. IEEE, 2020, pp. 2310–2316.